

# Annual Review of Fluid Mechanics Filtration in Pore Networks

## Linda J. Cummings,<sup>1</sup> Binan Gu,<sup>2</sup> and Lou Kondic<sup>1</sup>

<sup>1</sup>Department of Mathematical Sciences, New Jersey Institute of Technology, Newark, New Jersey, USA; email: linda.cummings@njit.edu

Annu. Rev. Fluid Mech. 2026. 58:221-44

The  $Annual\ Review\ of\ Fluid\ Mechanics$  is online at fluid.annual reviews.org

https://doi.org/10.1146/annurev-fluid-112723-054759

Copyright © 2026 by the author(s). All rights reserved

## **Keywords**

filtration, pore networks, Hagen-Poiseuille, fouling

#### **Abstract**

In liquid filtration, a particulate-laden feed solution is passed through a porous material (the filter), often a membrane, designed to capture the particulate matter. Usually, the filter has a complex interior structure of interconnected pores, through which the feed passes, and in many cases of interest, it may be reasonable to approximate this interior structure as a network of interconnected tubes. This idea, which dates back about 70 years, greatly simplifies the modeling and simulation of the filtration process. In this article, we review the use of networks as a framework for modeling and investigating filtration, describing the key ideas and milestones. We also discuss some promising areas for future development of this field, particularly concerning the design of next-generation filters.

<sup>&</sup>lt;sup>2</sup>Department of Mathematical Sciences, Worcester Polytechnic Institute, Worcester, Massachusetts, USA

#### 1. INTRODUCTION

Filtration—loosely speaking, the separation of particles from fluids—is a ubiquitous process, occurring in natural, household, biomedical, and industrial realms, on many different spatial scales. In nature, rain and groundwater are filtered by porous rocks and soil, and our own bodies carry out a wide range of filtration processes; in the household, we have water filters, coffee makers, tea strainers, air cleaners, and air-conditioning units, all of which rely on filtration; in the healthcare setting, filtration occurs during the use of medical masks, dialysis machines, ventilation, and anesthesia; and in industry, filtration is widespread in the manufacture of foods, drinks, and pharmaceuticals, among countless other areas. In most cases, the objective is either to remove undesired particles from a contaminated fluid (usually referred to as the feed solution in the industrial context) to clean it or to retain desired particles for use in some application. Filters operate on the broad principle that a particle-laden feed (liquid or gas) is passed through a porous material, with interconnected pores that retain the particles. Before discussing and reviewing in detail in subsequent sections how filtration can be effectively modeled in the context of pore networks, we first give a brief overview of the key factors and processes that must be taken into account (for a comprehensive discussion of various aspects of filtration, the reader is referred to van Reis & Zydney 2001, 2007; Iliev et al. 2015; Iritani & Katagiri 2016; Sparks & Chase 2016).

There are many different filter designs, but they often have common features. The simplest type of filter is a sieve or strainer, which usually consists of some mesh through which the feed is passed. The filtration principle here is rather basic: Particles too large to pass through the holes in the mesh will be retained by it (size exclusion), so that only the upstream surface of the sieve plays a role in the filtration. This type of filter is typically used only for relatively large particles (of the order of 100 µm or more) and is not discussed in this review. Most filters in widespread use are made of porous materials, often membranes, with a heterogeneous internal pore structure (see Figure 1 for some examples) that plays an important role in the filtration process. In contrast to simple sieves, such depth-structured filters can capture particles via a variety of distinct mechanisms, making them more effective at removing impurities. We introduce these particle-capture mechanisms shortly, but first we discuss fluid dynamics and the pore structure of the filter.

For filtration to be accomplished, the fluid in which the particles are suspended must be able to pass through the filter membrane, which presupposes either that pores are interconnected or that each individual pore forms a direct path from upstream to downstream surfaces. There are filter membranes that fall into this latter category—so-called track-etched membrane filters, two examples of which are shown in **Figure 1**e, f (in fact, the filter membrane in **Figure 1**e is really in both categories)—and this class of filters has received significant attention in the literature, due in large part to the simple structure, which makes for easy modeling. However, such filters are not in widespread use, and we focus here on the former type.

The details of fluid transport through a porous material are very different according to whether the material is saturated or (partly) dry. Both cases are important in applications, but our review focuses on the former case (for those interested in the latter regime, see, for example, Ridgway et al. 2002, Schoelkopf et al. 2002, Abdallah et al. 2023). When considering flow through porous media with interconnected pores, two important concepts are porosity, simply the void fraction of the porous material (usually denoted by  $\phi$ ), and permeability, a measure of the ease with which a fluid can flow through a material (usually denoted by k). Readers are referred to Probstein (1994) and references therein for an in-depth discussion of these concepts, including empirical relations (such as the Kozeny-Carman equation) between the two that may hold for certain types of porous media. Permeability is a more sophisticated measure than porosity, encapsulating information about the size, shape, and connectivity of the pores in the medium. Both quantities can be defined

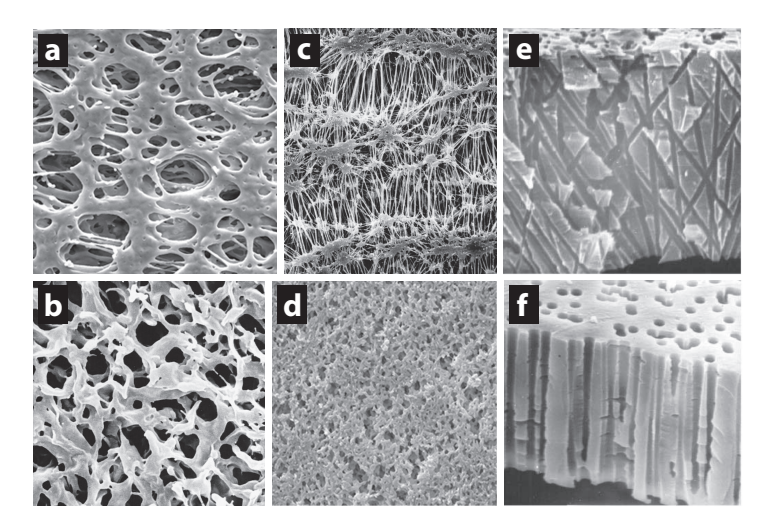


Figure 1

Enlarged images showing the pore structure of a selection of real filter membranes: (a) Express® PLUS (Millipore Sigma, pore size  $\sim$ 0.2  $\mu$ m), (b) Durapore® (Millipore Sigma, pore size  $\sim$ 0.4  $\mu$ m), (c) Fluoropore® (Millipore Sigma, pore size  $\sim$ 1.4  $\mu$ m), (d) nylon membrane (Millipore Sigma, pore size  $\sim$ 0.5  $\mu$ m), (e) track-etched polycarbonate membrane (pore diameter  $\sim$ 0.2  $\mu$ m), and (f) track-etched polypropylene membrane (pore diameter  $\sim$ 0.2  $\mu$ m). Panels a-d reproduced with permission from Millipore Sigma (https://www.sigmaaldrich.com/). Panels e and f reproduced from Apel (2001).

either globally, across the entire porous medium, or locally, either at the pore scale or by focusing on a representative local volume that is large compared with the pore size but small compared with the overall dimension of the porous material. While porosity is dimensionless, permeability has dimensions of length squared (an area) and is a material proportionality constant in the well-known empirical Darcy's law (Darcy 1856) (see the sidebar titled Darcy's Law, Pore Velocity, and Superficial Velocity).

As is clear from **Figure 1**, the interconnected pore structure may be very complicated, making quantitative modeling a challenge. Undaunted, some researchers use sophisticated image processing together with computational fluid dynamics tools (Blunt et al. 2013, Wiegmann 2024) or even deep learning methods (Wang et al. 2021) to simulate fluid flow, as well as particle transport and deposition, in detailed pore geometries. However, such approaches can be extremely computationally demanding, and the results are highly specific to a particular situation. For broad investigative applications such as exploring and optimizing filter design, simpler models that represent the interior pore structure of the filter as a network of pores, each of which individually has a simple geometry, can be very valuable.

The idea of representing interconnected pores of a porous medium as a network appears to have been first considered by Fatt in a PhD dissertation at the University of Southern California, subsequently published in 1956 as a three-paper series in *AIME Petroleum Transactions* (Fatt 1956a,b,c). Fatt argues that a network of cylindrical tubes is the simplest representation of a general porous medium with interconnected pores that can capture the key features of flow through such structures while retaining analytical tractability. Prior to Fatt's analysis, popular models for porous media included the bundle-of-tubes model and the sphere-pack model, each discussed in some detail by Fatt and also more recently by Esser et al. (2021) (both of which include appropriate historical references). As the name suggests, the former model represents pores as a bundle of disjoint tubes; although tractable (like the many models for track-etched

## DARCY'S LAW, PORE VELOCITY, AND SUPERFICIAL VELOCITY

In the flow of (Newtonian) viscous fluid through saturated porous media, two velocity measures are commonly considered: the pore velocity and superficial velocity.

## Pore Velocity upore

This is the actual velocity of fluid inside a pore, obtained by solving the Navier–Stokes equations inside the pore subject to no-slip boundary conditions at the pore wall and suitable pressure/flow conditions at the pore inlet/outlet.

## Superficial Velocity us

This is obtained by averaging the pore velocity over a control volume (consisting of solid material plus pores) that is large compared with the pores but small compared with the overall dimension of the porous medium. The superficial velocity and pore velocity are generally assumed to be related via the porosity:  $\mathbf{u}_s = \phi \bar{\mathbf{u}}_{pore}$  (where the overbar denotes a spatial average over an individual pore or some other suitable control volume).

## Darcy's Law

Darcy's law is a well-known empirical law stating that the superficial velocity of the fluid is directly proportional to the applied pressure gradient in a porous medium:

$$\mathbf{u}_{\mathrm{s}} = -\frac{k_{\mathrm{s}}}{\mu} \nabla p, \qquad \qquad \mathrm{SB1}.$$

where  $\mu$  is the dynamic viscosity and  $k_s$  is the permeability of the medium (Probstein 1994, Bear 2013). For sufficiently simple pores (such as simple cylindrical tubes) it may also be applicable on the scale of an individual pore,

$$\bar{\mathbf{u}}_{\text{pore}} = -\frac{k_{\text{pore}}}{\mu} \nabla p,$$
SB2.

in which case  $k_s = \phi k_{pore}$ .

membrane filters), this model is an oversimplification for most real porous media. The latter model represents the solid fraction of the porous medium as a collection of packed spheres, and it forms the basis for the well-known Kozeny–Carman equation, an empirical relation between the porosity of a porous medium and its permeability to flow (see Probstein 1994 and Bear 2013, and references therein). While certainly geometrically and conceptually simple, for the purpose of pore-scale fluid flow calculations, the sphere-pack model lacks tractability and, moreover, does not provide a quantitatively accurate description of most real porous media; thus, it does not offer any obvious advantages over the proposed network model in the general setting.

Fatt offers convincing evidence for the reasonableness and widespread applicability of the network model for porous media (see the sidebar titled Appropriateness of the Network Representation). Though it took some time for the ideas to gain traction, in the decades since his original work, they have proved very influential. Readers are referred to, for example, work by Simon & Kelsey (1971) and Rege & Fogler (1987), who build substantially on Fatt's work, as well as the recent study by Esser et al. (2021), where it is discussed at length and verified experimentally. In the late 1990s and onward, motivated by applications in the petroleum industry, groups such as that of M. Blunt advanced and popularized the approach, combining data from detailed micro–computed tomography (CT) 3D scans of porous materials with network-generation algorithms to produce relatively simple pore network representations [see the review by

#### APPROPRIATENESS OF THE NETWORK REPRESENTATION

Given some of the images in **Figure 1**, one may ask, How applicable are idealized network representations of the type shown in **Figure 2**? Clearly, in cases where the pores have a small aspect ratio, such as in **Figure 1**e, f; and perhaps in the porous medium of **Figure 2**b, the approach is reasonable. In more general cases, it is found that a network model can provide an acceptable approximation provided the pore topology and conductances are represented with good accuracy (Fatt 1956a,b,c; Blunt et al. 2013; Esser et al. 2021). For example, in the earliest model (Fatt 1956a,b,c), each distinct network is characterized topologically by its so-called pore connection index  $\beta$ : the number of other edges (pores) to which each edge (pore) is connected ( $\beta = 6$ , 4, 7, and 10 for the four network types shown in **Figure 2**c). Despite the simplicity, this pore network model was shown to provide quite good agreement with results for flow through real porous media for measures including network permeability and resistivity (Fatt 1956c, Esser et al. 2021), provided the  $\beta$ -value is matched to the average value for the medium and the pore-size distribution is appropriately matched (see also the sidebar titled Choosing the Pore-Size Distribution).

Blunt et al. (2013), and references therein]. In contrast to Fatt's work, which was limited to simple regular network patterns, such data-based approaches allow a network representation to be extracted from an arbitrary porous medium, provided a well-resolved 3D image can be obtained.

Network representations of porous media offer significant advantages in terms of analytical tractability and the ability to quickly compute flow through the medium, critical for the applications in oil recovery that motivated the original work (Fatt 1956a,b,c). For the filtration applications that are our focus here, we must also consider the processes by which particles in the fluid are carried through and deposited in the pore network. Particle capture by the pores of the filter is synonymous with fouling of the filter. Such fouling alters the pore structure, ultimately degrading filter performance; once a filter is heavily fouled, it is no longer effective and must be replaced or cleaned (Sparks & Chase 2016). First, and usually most important among the particlecapture mechanisms, depth-structured filters can capture particles that are much smaller than the pores via adsorption at pore walls. Particles carried by the flow encounter a pore boundary and stick to it with some nonzero probability, possibly due to electrostatic interactions. This type of fouling, known as adsorptive or standard fouling, leads to pore shrinkage over time and increased resistance of the filter to flow through it. The next type of capture mechanism is when particles of size comparable to the pores get stuck in a pore, leading to total (or partial) occlusion of that pore. This filter fouling mechanism is accordingly known as complete (or partial) blocking. It may occur at interior points of the filter or at the upstream surface. In the latter case, it is a type of sieving and is a precursor to the final type of filter fouling mechanism: so-called caking. In caking (which usually occurs at a late stage of the filtration when the filter is already heavily fouled), particles begin to accumulate on the upstream surface of the filter as a cake layer.

With the key ideas in place, we now describe in more detail the concepts that underpin filtration in pore networks.

## 2. PORE NETWORK GENERATION

If one is to have a realistic network representation of a porous medium, one needs robust ways to generate representations that preserve the features essential for accurate modeling and predictions. Broadly speaking, two approaches to this challenge are commonly used: (a) start with the pore space of an existing porous medium and attempt to reduce it to the closest analogous network or (b) generate artificial networks that are representative of typical porous media for the application considered.



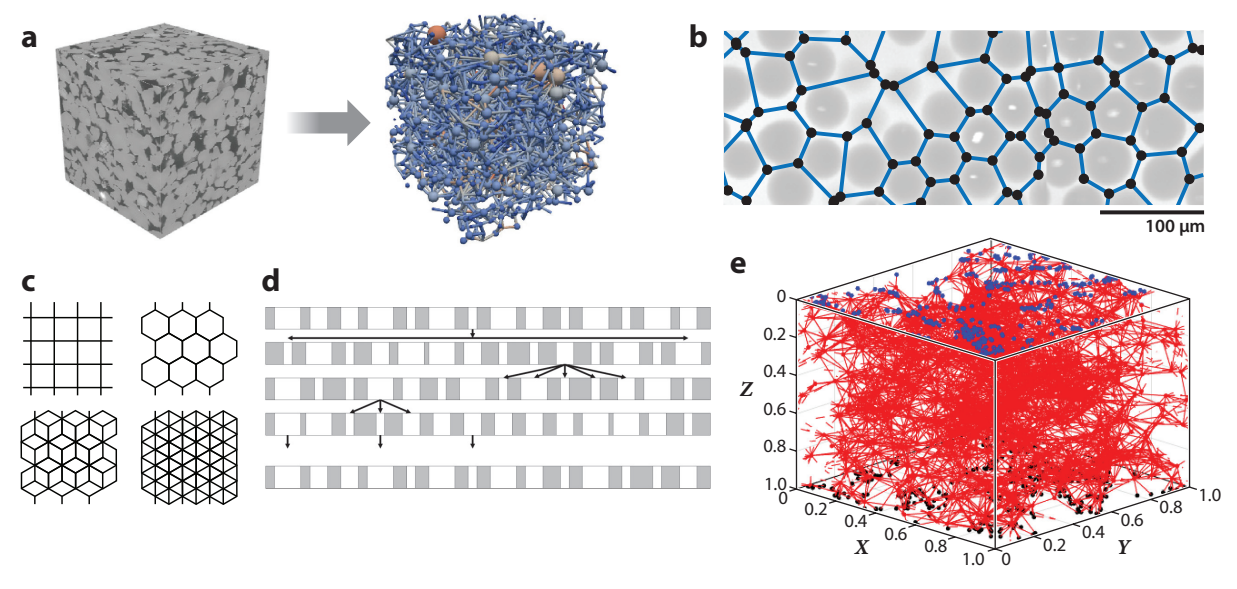


Figure 2

Examples of network representations of porous materials. (a) Schematic illustrating the process by which an idealized network (right) is extracted from an image of a real structure (left; here a porous sandstone sample). (b) Pore skeleton used by Kelly et al. (2023) to model flow in the pores between packed glass beads. (c) The four regular pore networks introduced by Fatt (1956a). (d) Semiregular layered pore network (white represents pore space and gray is solid membrane) (Beuscher 2010). (e) Artificially generated pore networks (Gu et al. 2022b) used to investigate membrane filter design. The image shows a section of a membrane, with blue dots representing pore inlets on the upstream membrane surface, black dots showing pore outlets on the downstream surface, and red lines indicating interior pores (the edges of the network). Panel a adapted from Gong et al. (2020) (CC BY 4.0). Panel b reproduced with permission from Kelly et al. (2023). Panel c modeled after concepts presented in Fatt (1956a). Panel d reproduced with permission from Beuscher (2010).

In the former approach, the work of Blunt and coworkers, though developed in the context of geological modeling rather than filtration, is especially noteworthy [see the comprehensive and impactful review article by Blunt et al. (2013) and the many references therein]. In this context, another useful and influential review that presents an alternative perspective is that of Xiong et al. (2016). Blunt's group is at the forefront of so-called digital core analysis, which analyzes 3D images of real porous media to extract useful physical information. Images are typically generated using X-rays (micro-CT scan) or focused ion beams (scanning electron microscopy), then binarized into regions of solid material and empty space (void). Once this is done, there are well-developed techniques by which one can identify the larger voids (pore junctions, usually modeled as spheres in this approach) and the narrower pore throats that connect them (modeled as cylindrical tubes). The volumes of the spheres and tubes can be inferred by matching to the volume of the imaged pore space. This process is schematized in Figure 2a. Other groups have used similar approaches, e.g., Jiang et al. (2007), Abdoli et al. (2018), Kelly et al. (2023), and Shi et al. (2025); Figure 2b shows an example from Kelly et al. (2023) where flow through a low-porosity structure comprising packed glass beads is considered. In this particular study, the authors proceed by imaging a 2D cross section of their experiment and using that image to extract the pore network (referred to as the pore skeleton in the context of porous media) of cylindrical tubes. Despite the quasi-2D nature of the model, it can reproduce the experiments remarkably well.

The latter approach, of generating artificial pore networks, is useful for filter design exploration. When coupled with the type of efficient modeling and simulation techniques described in

Section 3, a wide range of different pore networks can be explored to identify those that perform optimally in a given filtration scenario. Artificial pore networks are generated in two stages: One first constructs the pore skeleton, which fixes the pore axes (the edges of the network); then one prescribes the cross-sectional shape of the pores about the axes (often a simple circular cylinder, though the model easily extends to other pore shapes, provided they are slender). We describe the first step by way of examples below, before considering the second.

Infinitely many unique networks exist, of course, but a few broad classes commonly considered in the context of flow through porous media may be distinguished. Regular networks, which have a basic subunit that repeats periodically, are the simplest type and, not surprisingly, were the first to be considered as models of porous media. Fatt (1956a) studied four basic regular pore networks, reproduced in **Figure 2***c*: a square network and single, double, and triple hexagonal networks (the double and triple hexagonal networks are obtained by superimposing either two or three copies of the single hexagonal network). Though the pore skeletons lie in a plane, each edge in the network represents a circularly cylindrical 3D pore (cf. Kelly et al. 2023).

Next (in roughly increasing complexity) are networks that have a predictable, but nonrepeating, structure, such as the tree-type pore networks considered by Gu et al. (2020) (see also Sanaei & Cummings 2018). While simple to classify and analyze, such structures do not make good filters, performance being limited by the small number of pore inlets, which quickly clog. More robust in terms of performance, and only slightly more complex, are filters with pore networks that might be described as semiregular, exemplified by layered networks of the type considered by Beuscher (2010) and Krupp et al. (2017), where the number of pores in each layer is drawn from a random distribution (see **Figure 2d**).

Finally, efficient solution methods and modern computing power mean that the processes that govern filtration can be simulated even on large, random pore networks, provided the pores are cylindrical (or nearly so). Several groups use variants of the random geometric graph to generate networks, such as that shown in Figure 2e. Griffiths et al. (2020) construct networks within a square prism that represents a chunk of membrane filter material and assign the numbers of pore inlets, pore outlets, and interior pore junctions (vertices of the network). The associated points are placed randomly on the upstream surface, on the downstream surface, and in the prism interior, respectively. The choice of which junctions are connected by pores is decided by assigning a maximum pore length, d (which may vary spatially for a heterogeneous filter), and joining all vertices closer than d by a cylindrical pore. Gu et al. (2022a,b) take a similar approach but avoid the issue of assigning the number and locations of inlets and outlets by starting with a prism that is twice as thick as the membrane. They generate a network using the same maximum pore length protocol (here implemented with a doubly periodic connection metric across the s and y directions, indicated by dashed lines in the example of Figure 2e, then cut along planes equidistant from the membrane midsection, in the process automatically generating inlets and outlets where pores are cut. [Inhomogeneous networks can be created by implementing this protocol with appropriate probability distributions governing where vertices are placed (Gu et al. 2023) or by varying the value of the connection distance d throughout the region (Griffiths et al. 2020).]

With pore skeletons such as those in **Figure** 2*c*–*e* generated, the next step is to expand each edge of the network to a 3D pore. The simplest way to do this, and the most widely adopted in this context, is to assume that pores are circular cylinders. Each edge of the network is then the axis of a surrounding pore, the radius of which must be assigned. Approaches to assigning pore radii vary (see the sidebar titled Choosing the Pore-Size Distribution), ranging from setting all radii to the same constant value (Fatt 1956b, Griffiths et al. 2020, Gu et al. 2022a), to using selected probability distributions (Fatt 1956c, Johnston 1998, Iliev et al. 2015, Gu et al. 2022b) intended

#### **CHOOSING THE PORE-SIZE DISTRIBUTION**

In modeling a porous material as a network, there are multiple approaches to assigning the pore sizes.

## **Image-Based Methods**

If one follows a network-extraction protocol based on analyzing images of a real medium (cf. Blunt et al. 2013), this will lead to a pore skeleton with edges  $e_{ij}$  joining vertices  $v_i$  and  $v_j$ , fixing pore lengths  $\ell_{ij}$ . Within this framework, the same image analysis tools allow pore volumes  $\operatorname{Vol}_{ij}$  to be estimated, from which radii  $r_{ij}$  follow  $(\pi r_{ij}^2 \ell_{ij} = \operatorname{Vol}_{ij})$ . Since porosity is strongly correlated with filtration efficiency (Gu et al. 2022a), we recommend an a posteriori check that the resulting pore network porosity matches that extracted by the image analysis software and scaling all pore radii uniformly, if necessary, to achieve the same precise value.

#### **Distribution-Based Methods**

Alternatively, pore sizes may be chosen from an appropriate probability distribution. Fatt (1956c) took this approach in his original work, choosing to select pore radii randomly from a discrete frequency distribution [in Fatt's approach, although regular networks are used, pore (edge) lengths are assumed inversely proportional to pore radii]. The most appropriate distribution to use for pore sizes has been studied by several authors [see in particular Zydney et al. (1994) and the review by Johnston (1998), and references therein].

> to mimic those in real porous media, to assigning different pore radii in different regions of the medium (Gu et al. 2023).

#### 3. FLUID DYNAMICS IN PORE NETWORKS

With a pore network in hand, the next step is to model and simulate the fluid flow through it relevant for filtration scenarios. In this section, we review and discuss the most widely used approaches to modeling flow through pore networks in permeable filter materials.

## 3.1. Computational Fluid Dynamics Modeling

Our focus in this review is on porous media modeled by networks of cylindrical, or near-cylindrical, pores, with a key aim being to circumvent the need for intensive computations. Nonetheless, since many practitioners use computational fluid dynamics (CFD) methods (broadly interpreted) in filtration modeling, a few remarks can be made. CFD-based approaches are used primarily when solutions are computed on complicated domains, typically those arising from direct 3D imaging techniques. In industry, researchers often make use of commercial software packages to solve for flow (and particle transport/deposition) through complicated 3D real pore structures. One popular such package is GeoDict (Wiegmann (2024), with a flow solver based on the lattice Boltzmann method (Chen & Doolen 1998), developed at the Fraunhofer Institute for Industrial Mathematics and now used by a range of industries, national labs, and universities. Such packages offer several advantages, including the ability to process supplied images of 3D porous media, convert them to digitized flow domains with high resolution, and solve the Navier-Stokes equations for fluid dynamics through the resulting structures. Thus, software such as this is well-suited to analyzing the performance of existing filters (and other porous materials used in fluid dynamical applications) under different scenarios. It is not, however, suited to investigations relating to optimizing filter design, since the computational cost to test the performance of many different pore structures is prohibitive, nor is it well-suited to simulating large-scale filtration over long times. Moreover, even if the chosen software is able to resolve the details of the flow with high accuracy, the fidelity of the



filtration simulation relies on a specific choice of assumptions about how particles are transported and deposited within the porous medium (see the discussion in Section 4). So CFD simulations are still limited by the appropriateness of the mathematical fouling model.

The interested reader is referred to the review by Iliev et al. (2015) for extensive discussion of CFD-based methods in filtration modeling (see also Xiong et al. 2016). With the growth in popularity and the recent advances that have been made in artificial intelligence (AI) and machine learning (ML), AI/ML-based approaches are now showing promise for predicting important properties of porous materials such as permeability, often in conjunction with tools such as GeoDict (Griesser & Fingerle 2020, Wang et al. 2021, Caglar et al. 2022). We anticipate that in the near future, AI/ML methodology will also prove to be a powerful way to augment large network flow models (see Section 6 for further discussion).

## 3.2. Network Modeling Basics: Hagen-Poiseuille Flow Resistor Model

Our focus here is on filter materials where the pores may be considered to have a true network structure embedded in 3D space (see, e.g., **Figure 2***a*,*e*). Whether modeling a hypothetical porous material or a real one, the assumption is that there are clearly identifiable pores that are analogous to the edges in the network and pore junctions at which two or more pores connect, analogous to the nodes.

A fundamental principle in modeling the flow of a Newtonian fluid (viscosity  $\mu$ ) through a saturated network of pores is that it is entirely analogous to the flow of current through an electrical circuit, with each pore in the network playing the role of an electrical resistor (see, e.g., Zhang & Hoshino 2018, chapter 3). Consider first a single pore, which admits a volumetric fluid flux Q under a pressure difference  $\Delta P$ . The analog of Ohm's law V = IR that relates electrical current I through a circuit with a single resistor of resistance R, to the potential difference V across it, is  $\Delta P = QR$ , where R is the resistance of the pore. Some authors prefer the concept of pore conductance, K = 1/R (closely related to permeability), in terms of which Ohm's law is written as  $Q = K\Delta P$ .

In the special case where we assume the pore is a circular cylinder of radius  $r_0$  and length  $\ell$ , through which flow is steady and unidirectional, the pressure gradient along the pore is constant, and the speed  $u_{\text{pore}}$  is given by the Hagen–Poiseuille solution (for an interesting historical overview, see Sutera & Skalak 1993)

$$u_{\text{pore}} = \frac{\Delta P}{4u\ell} (r_0^2 - r^2),$$
 1.

where r is a local radial polar coordinate centered at the pore axis. The underlying assumptions will be approximately satisfied provided the Reynolds number for the flow is not too large, so that flow is laminar, and  $\epsilon = r_0/\ell \ll 1$ , so that the pore is sufficiently slender for the unidirectional Hagen–Poiseuille flow to be fully developed along most of its length. Averaging across the pore and comparing with the pore-scale Darcy's law (Equation SB2) (here considered as a simple scalar equation), we find

$$\bar{u}_{\text{pore}} = \frac{(\Delta P)r_0^2}{8\mu\ell} = \frac{k_{\text{pore}}(\Delta P)}{\mu\ell},$$
 2.

giving  $k_{\text{pore}} = r_0^2/8$  as the permeability of a circularly cylindrical pore of radius  $r_0$ . The flux down the pore is  $Q = \bar{u}_{\text{pore}}A = \pi(\Delta P)r_0^4/(8\mu\ell)$ , from which we obtain the pore resistance and conductance as

$$R = \frac{8\mu\ell}{\pi r_0^4}, \quad K = \frac{\pi r_0^4}{8\mu\ell}.$$
 3.

www.annualreviews.org • Filtration Networks

Note that these formulae allow the Reynolds number for the pore (based on pore length) to be estimated a posteriori as  $\text{Re}_{\text{pore}} = \rho(\Delta P)r_0^2/(8\mu^2)$ , where  $\rho$  is the fluid density. In most filtration scenarios  $\text{Re}_{\text{pore}}$  will never approach values that could trigger turbulence.

From these basic building blocks, we can readily construct the fluid dynamical model for flow through an arbitrary network of interconnected cylindrical pores in 3D space. Formally, the ideas extend to pores that are noncylindrical, provided they are nearly so, and in practice the model applies in situations where pores are far from cylindrical, provided their conductance can be appropriately characterized (see the sidebar titled Appropriateness of the Network Representation). Suppose for definiteness (and in line with most relevant filtration literature) that the porous material, and therefore the pore network, occupies a slab between two parallel planes, which form the upstream and downstream sides of the filter when it is operational. Pores (network edges) intersect the upstream (top) plane at inlets and the downstream (bottom) plane at outlets (special cases of nodes in the network). We assume that the vertices  $v_i \in V$  of the network are enumerated via an integer index i and that some subset of the vertices are connected, such that  $e_{ij} \in E$  is the edge connecting  $v_i$  and  $v_j$ . Vertices correspond to pore junctions and edges to the connecting pores; V and E are the vertex and edge sets, respectively. Pore lengths  $\ell_{ij}$  are then determined by the Euclidian distance between  $v_i$  and  $v_j$ , while pore radii  $r_{ij}$  must be assigned (see the sidebar titled Choosing the Pore-Size Distribution).

The fundamental information on the connectivity of a network is encoded in its adjacency matrix  $A_{ij}$ , which records (via unit entries) which vertices (i,j) are connected (all other entries are zero). To describe the fluid dynamics of the pore network, we need a weighted version of this adjacency matrix, the conductance matrix,

$$K_{ij} = \begin{cases} \frac{\pi r_{ij}^4}{8\mu\ell_{ij}} & e_{ij} \in E, \\ 0 & e_{ij} \notin E. \end{cases}$$
 4.

The flux  $Q_{ij}$  through the pore along edge  $e_{ij}$  is then  $Q_{ij} = K_{ij}(P_i - P_j)$ , where  $P_i$  is the pressure at node i.

The pressures at the membrane's top and bottom surfaces must differ to drive fluid flow through the pore network. Two scenarios are typically considered: constant pressure and constant flux. In the former, the pressure difference across the membrane is prescribed; in the latter, due to membrane fouling, the pressure difference must increase over time to maintain the constant flux. We outline the constant pressure implementation below.

At each interior vertex, conservation of fluid flux  $Q_{ij}$  from individual pores is imposed at nodal connections (the analog of Kirchoff's law in electrical circuits). More precisely, for each interior vertex  $v_i \in V_{\text{int}} \subset V$ , we obtain

$$\sum_{v_{j}: e_{ij} \in E} Q_{ij} = \sum_{v_{j}: e_{ij} \in E} K_{ij}(P_i - P_j) = 0,$$
5.

forming an algebraic system of equations for pressures at the interior vertices. This system admits a graph Laplacian structure (Gu et al. 2022a)

$$L_K P(v_i) = 0, \quad v_i \in V_{\text{int}}; \quad P(v) = \begin{cases} P_0 & v \in V_{\text{top}}, \\ 0 & v \in V_{\text{bot}}, \end{cases}$$
 6.

where  $V_{\text{top}}$  and  $V_{\text{bot}}$  denote the set of vertices on the top and bottom membrane surfaces, respectively (the inlets and outlets), and

$$L_K = D - K, \quad D_{ij} = \begin{cases} \sum_{l=1}^{|V|} K_{il} & j = i, \\ 0 & \text{otherwise.} \end{cases}$$
 7.

The construction of the (weighted) graph Laplacian matrix  $L_K$  follows a more rigorous approach, leveraging tools from linear algebra, function spaces on graphs, and discrete calculus; we refer the reader to the book by Grady (2010) for these details. Given a graphical input such as the conductance matrix K, solving the system in Equation 6 yields the pressures at interior vertices, which can then be used to compute fluid velocities/fluxes through each pore  $e_{ij}$  via the Hagen-Poiseuille solution, per Equations 1 and 2.

The constant flow condition can also be implemented in this setup. The applied pressure  $P_0$  becomes an unknown, and  $Q_{top}$ , the total fluid flux through the pore inlets, is prescribed, which provides the additional equation required to determine  $P_0$ ,

$$Q_{\text{top}} = \sum_{e_{ij}: v_i \in V_{\text{top}}} Q_{ij} = \sum_{e_{ij}: v_i \in V_{\text{top}}} K_{ij} \left( P_0 - P_j \right)$$

$$\Longrightarrow P_0 \sum_{e_{ij}: v_i \in V_{\text{top}}} K_{ij} - \sum_{e_{ij}: v_i \in V_{\text{top}}} K_{ij} P_j = Q_{\text{top}}.$$

Whichever scenario is considered, the solution, even for large networks with many thousands of vertices, is quick and efficient even when implemented on a simple platform such as MATLAB (The MathWorks Inc. 2024) [e.g., approximately 0.008 s to solve the system in Equation 6 with  $4\times10^3$  unknown pressures on a local desktop (12th Gen Intel® Core<sup>TM</sup>i5-12600K 3.70 GHz with 64G RAM)], to the extent that it is straightforward to gather statistics on the effect of random variations, either in the network structure or in the pore-size distribution (Gu et al. 2022b) (independent realizations of the distribution can be run in parallel). As a point of historical interest, we note that when (Fatt 1956b, p. 161) considered essentially the same system in 1956, he commented,

The network models used in this study lead to determinants of several hundred rows and columns; that is, determinants of order 100 or more. Such determinants cannot be evaluated by any reasonable amount of labor. Even modern high-speed computers cannot evaluate determinants of greater than 30th order unless the determinant has some symmetry condition that permits reduction to a lower order.

The means by which Fatt circumvented this obstacle were ingenious:

Networks of electrical resistors [with resistances proportional to the pore resistances] were constructed, and the total resistance was measured by a conventional Wheatstone bridge. The network of electrical resistors is, therefore, an analog computer which is used to solve network problems when these problems cannot be solved conveniently by analytical or numerical methods.

Though presented here in the context of a saturated porous filter medium, the theory outlined above is generally applicable to flow through any type of network that may be reasonably approximated by interconnected cylindrical pores (or indeed other pore shapes, provided one can appropriately characterize the conductances  $K_{ij}$ ) and is accordingly used in a wide range of applications (Gavrilchenko & Katifori 2018, Chang & Roper 2019, Ronellenfitsch & Katifori 2019, Konkol et al. 2022, Taira & Nair 2022).

## 4. FOULING OF PORE NETWORKS

For the specific filtration application considered here, it is critical to account for the fact that the pore network evolves in time due to fouling (for a comprehensive discussion, see, e.g., Iritani & Katagiri 2016). Such evolution may be continuous in time, as is the case with the adsorptive fouling that we discuss first below, or discrete, as with the sieving discussed subsequently. In modeling filtration, one is usually interested in identifying scenarios or filter designs that lead to improved

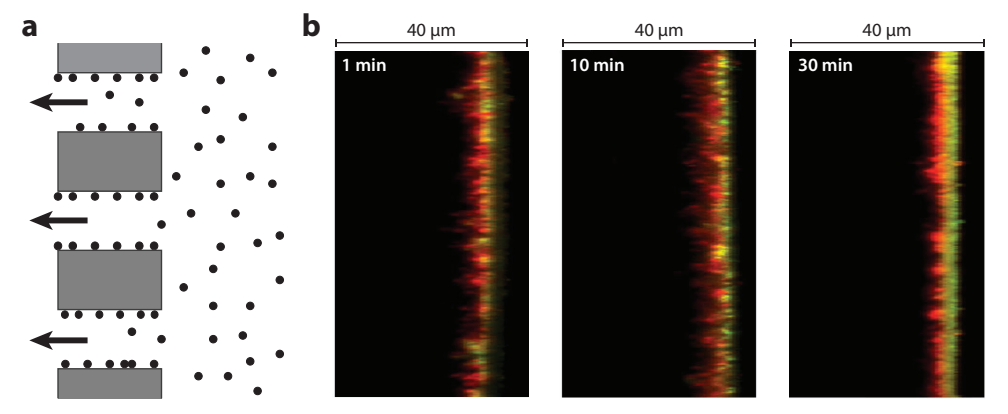


Figure 3

(a) Schematic illustration showing adsorptive fouling of pore interiors due to particles much smaller than the pores (arrows show the direction of filtrate flow). (b) Experimental time-lapse images of a membrane filter (filtration takes place from right to left) showing adsorptive fouling by two types of fluorescently labeled nanoparticles. Panel b adapted from Fallahianbijan et al. (2017).

performance over the filter lifetime. To this end, model simulations must typically be run through the late stages of filtration until fouling has progressed sufficiently that the filter is deemed no longer useful.

## 4.1. Small Particles: Adsorptive Fouling

The most prevalent and relevant (from the point of view of filter performance deterioration) type of fouling is adsorptive fouling due to particles smaller than the pores depositing on pore walls, shrinking them (see Figure 3). Since the resistance of each pore is inversely proportional to the fourth power of the pore radius (Equation 3), such fouling is very consequential for the energy requirements of filtration. Adsorptive fouling has been considered extensively at the level of individual pores; in the following, we focus mainly on the network-specific modeling literature, referring the reader to other sources and references therein for a more general overview (Iliev et al. 2015, Iritani & Katagiri 2016, Sparks & Chase 2016, Tanudjaja et al. 2022). How the particle transport and adsorption (deposition) are modeled depends on the assumptions made about the relative importance of advection and diffusion on the transported particles, a key parameter being the particle Péclet number based on axial flow along the pore, Pe =  $U\ell_0/D$ , where U is a typical value of the flow (pore) velocity [characterized by  $U = r_0^2 \Delta P/(\mu \ell_0)$  for a pore of radius  $r_0$ and length  $\ell_0$  under a pressure drop  $\Delta P$  and D is the diffusion coefficient of the particles in the feed fluid. In general, it is reasonable to assume a quasi-steady model for particle transport since the timescale of interest is that on which the membrane fouls, which is much longer than typical transit times for individual foulant particles. An appropriate strategy, then, is to solve a quasisteady model for the concentration of the small foulant particles throughout the pore network, then couple this to an evolution equation for the local pore radius and proceed iteratively.

The simplest models assume passive (advection-dominated) transport of particles along the pore axis. Such models are reasonable provided that the axial Péclet number Pe defined above is large, which it is for many cases of interest in the Hagen–Poiseuille flow regime. If the Péclet number based on the pore radius,  $Pe(r_0^2/\ell_0^2)$ , is simultaneously small (Sanaei & Cummings 2017, Kiradjiev et al. 2021), this simply has the consequence that diffusion is rapid in the pore radial direction, so that the particle concentration is more or less uniform over the pore cross section,

#### ADDITIONAL FACTORS AFFECTING ADSORPTIVE FOULING

Most models for adsorptive fouling assume that the interactions between particles and the membrane pore wall that are responsible for fouling are fixed for a given feed/membrane system. In reality, however, once filtration has begun and the clean membrane begins to foul, the foulant layer that builds up on the interior pore walls shields the membrane from interacting directly with foulant particles. This shielding effect is well-known (Boussu et al. 2006, Iliev et al. 2015, Sparks & Chase 2016, Park et al. 2018, Zhang et al. 2020, Song et al. 2025) but not often considered in modeling, perhaps due to difficulty in characterizing it. Since network models of the type described above track the local thickness of the fouling layer via the particle deposition model adopted, one could attempt to incorporate shielding into a network model by, for example, making the deposition rate a function of the local foulant layer thickness.

For filtration of dense suspensions, particle–particle interactions are also important and should be taken into account. This will require modifications to both the transport model and the particle deposition law.

but advection still dominates transport along the axial direction. Other authors, e.g., Kim & Liu (2008) and Liu et al. (2020), have commented on the importance of diffusion (including possible shear-induced diffusion relevant for concentrated suspensions; see Leighton & Acrivos 1987a,b) and have proposed more complete models for the particle transport, relevant in regimes where filtration is slow and/or the pores are extremely small. Even with diffusion included, however, the problem may be simplified by averaging over the pore cross section, leading again to a 1D model along the pore axis (Liu et al. 2020). The physical effects one chooses to include in the particle transport model determine the complexity of the equations to be solved within each pore, with implications for computational demands on large networks. Some additional considerations that may be important are discussed in the sidebar titled Additional Factors Affecting Adsorptive Fouling.

Particle deposition at the pore wall may be accounted for in a number of ways, for example, by a simple probabilistic law (e.g., Iritani & Katagiri 2016, Griffiths et al. 2020) or by a sink term in the axial advection equation for the particle concentration (e.g., Sanaei & Cummings 2017, 2019; Gu et al. 2020, 2022a). In either case, the selected deposition model is intended to capture relevant physics, such as electrostatic interactions between the transported particles and the membrane material that composes the pore walls (Iliev et al. 2015, Sparks & Chase 2016, Tanudjaja et al. 2022).

The chosen particle transport/deposition model must be solved on the network. Since the flow is already solved and the particle transport problem is quasi-static, the challenge is to solve a 1D first-order (advection only) or second-order (advection and diffusion) differential equation for the particle concentration within each pore of the network as a function of the distance along the pore axis, with coupling between pores imposed via suitable continuity conditions at nodes. Particles removed from the flow deposit on the walls, shrinking them locally according to a simple mass conservation condition. In the most general case, solving this model (coupled differential equations on each edge of the network, which have to be solved at each time step as the pores shrink) can be computationally intensive, given that pore networks relevant to many filtration scenarios are typically large and that a desired goal is to investigate networks that optimize filter design (which requires that the model be solved until the filter is no longer useful). This motivates the search for appropriate simplifications that reduce computational demands.

If one neglects diffusion and assumes cylindrical pores, then the problem can be solved quickly and efficiently: For a sufficiently simple advective transport law, the particle concentration may



be obtained exactly, and the problem is reduced to a matrix system for the particle concentration values at the nodes of the network (Gu et al. 2022a). A typical full simulation, run up to flux extinction (one of many possible termination criteria) for adsorptive fouling on a network with approximately 20,000 edges, using an explicit numerical method and a time step of 10<sup>-4</sup> dimensionless units, takes about 10 to 12 s [on a local desktop (12th Gen Intel® Core<sup>TM</sup> i5-12600K 3.70 GHz with 64G RAM)], a computational effort far cheaper than a full partial differential equation (PDE) solve, which can take up to 30 min on the same system. The price for this gain in simplicity and efficiency is some inconsistency: The particle concentration advection model leads inherently to a concentration profile that decreases along the pore axis. A consequence of this is that particle deposition on the pore wall decreases along the pore axis also, so the pores should shrink more rapidly at the upstream ends, becoming noncylindrical. A pragmatic compromise is to impose a mass conservation rule that shrinks each pore in a cylindrical fashion according to the total volume of particles deposited in the pore (Griffiths et al. 2020, Gu et al. 2022a). However, since the evolution of the pore geometry is not then accurately captured, this approach has the drawback that network resistance and filter lifetime will be incorrectly predicted, with implications for optimization. In their investigations, Gu et al. (2022a) found that errors incurred in using the cylindrical pore approximation are typically smaller than 10% for all quantities of interest. More accurate results could be obtained efficiently by implementing models that approximate the noncylindrical pore evolution while still respecting mass conservation. For example, the authors have conducted a preliminary study of a model that allows pores to evolve as sections of circular cones, which shrink faster at the upstream ends (due to the higher impurity concentrations there), finding that very accurate results can be obtained with essentially the same computing demands as the cylindrical pore model.

In addition to the construction of the algebraic system in Equation 6 for pressure, the computational convenience of having the graph Laplacian (as defined in Equation 7) in the setting of fouling is also worth highlighting. Regardless of the governing equations that model foulant transport, setting up conservation of particle flux at each network interior vertex utilizes the connectivity information encoded in the graph Laplacian. Such vertex conditions, when appended to the boundary conditions and governing equations in the graph edges (ordinary differential equations/PDEs), can be formulated as a differential-algebraic system of equations to represent the vertex quantities. In general, the solution of such differential equations lies in the realm of quantum graphs (see, for example, Berkolaiko & Kuchment 2013, Arioli & Benzi 2018, Brio et al. 2022). Recently, Goodman et al. (2024) developed a MATLAB-based computational package to solve PDEs on graphs, with visual aids, and other authors (Chang & Roper 2019, Ruiz-García & Katifori 2021, Lawrie et al. 2022) have demonstrated similar numerical approaches to solving systems on networks in other scientific contexts. Such works highlight the versatility of the weighted graph Laplacian in modeling fluid and species transport on networks.

## 4.2. Large Particles: Sieving/Blocking

If the feed solution also carries particles comparable in size to the pores (the pore radii in the network model), these may become lodged within the network when they encounter a pore too small to transit. Since these pores then become (either partially or totally) blocked, this form of fouling is often referred to as blocking in the literature (see Figure 4). In most membrane filtration applications, one would like to have small-particle adsorption (which makes much more efficient use of the filter's capacity) as the dominant fouling mechanism, so ideally, large particles would be removed in a prefiltration step. For this reason, blocking has been less studied than adsorption from a filtration perspective: readers are referred to the recent review by Marin & Souzy (2025) and the many references therein, as well as accessible articles by Dressaire & Sauret (2017) and

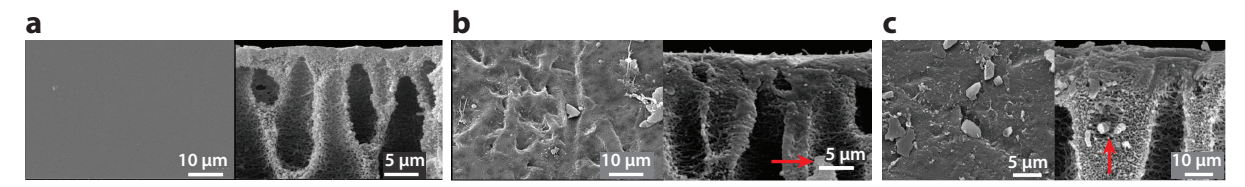


Figure 4

Experimental images illustrating the blocking and caking fouling modes. Here, panel *a* shows the clean filter; panels *b* and *c* show successive fouling levels. In each panel, the filter upstream surface is seen at the left, and the filter cross section is at the right. In panel *b*, large-particle blocking is evident on the filter surface and at the bottom right in the cross section (marked by the *red arrow*). In panel *c*, large blocking particles (*red arrow*) as well as a cake layer at the top are evident. Figure adapted from Chaipetch et al. (2021) (CC BY 4.0).

Dincau et al. (2023), for in-depth discussion of pore clogging by particles comparable to the pore size, in the broader context.

In a basic sieve such as one encounters in the kitchen, the process is very simple, but in a network of pores (particularly where there is a pore-size gradient; see Section 5.2), large particles may partially transit the membrane in a stochastic manner before blocking a pore. Predicting when and where this blockage occurs can be challenging. One of the earliest impactful studies was that of Rege & Fogler (1987), who introduce a network model of filtration that has large-particle blocking as the only fouling mechanism (adsorptive fouling is ignored). They use the basic flow network model introduced in Section 3.2 and assume that blocking particles are carried passively by the flow within a pore, executing a biased random walk through the network, with transition probabilities at pore junctions assigned according to the flux ratios in the outgoing pores. Note that in a simple blocking model of this kind, nontrivial results will be obtained only if one has a distribution of pore sizes. If all pores have the same radius, then either a particle is smaller than the pores and it will transit the membrane without being captured, or it is larger than the pores and will be trapped at the upstream surface of the membrane. Even if one includes adsorptive fouling also (see, e.g., Griffiths et al. 2014, Sanaei et al. 2016, Krupp et al. 2017, Liu et al. 2020), an initial distribution of pore sizes is still needed to obtain a blocking event at an internal pore of a pore network. This is because adsorptive fouling is greatest at the upstream membrane surface, so if all pores have the same initial radius, the inlet pores will always have the smallest radii for subsequent times. Internal blocking events can only occur in the event that pores in the membrane interior are smaller than inlet pores. As discussed in Section 5.2, many membrane filters are designed with such a negative pore-size gradient, which leads to more uniform fouling and extended filter lifetime. More sophisticated models that account for blocking with variable pore sizes, and indeed variable particle sizes also, have been presented [see, for example, work by Beuscher (2010) (from which **Figure 2***d* is taken) and by Krupp et al. (2017)].

While the network-based models described above provide a foundation for understanding particle transport and blocking in pore networks, simulating these dynamics in detail presents significant computational challenges due to the inherent stochasticity and complexity of the system. Given the inherent stochasticity of blocking dynamics, Monte Carlo methods are commonly used to estimate key performance metric statistics, often requiring many independent realizations (Marin & Souzy 2025). Additionally, for high large-particle arrival rates—corresponding to blocking-dominated filtration—accurately describing the underlying adsorptive dynamics often necessitates a small time step in temporal integration to resolve successive particle arrivals, further increasing computational complexity. Adsorption and sieving operate simultaneously in fouling, collectively altering the internal structure of the pore network. However, most models treat them

as independent processes. Future work could explore ways to more explicitly integrate these processes within unified network models, allowing for a deeper understanding of how adsorption and sieving might coevolve under different operational conditions.

## 4.3. Late Stages: Cake Formation

This type of fouling typically occurs only at a late stage of the filtration, when the filter's interior is already heavily fouled and filtration is inefficient. With fouling so heavy that particles cannot readily enter the pore network, a cake layer of particulate matter builds up on the upstream surface of the membrane (see **Figure 4c**). Due to the inefficiency of the filter, which provides extremely high resistance to the flow by this stage, it would normally be discarded or cleaned by the time this occurs. Nonetheless, some models of caking have been considered in the literature (Ho & Zydney 2000, Herterich et al. 2019, Sanaei & Cummings 2019, Köry et al. 2021, Pereira et al. 2021; for a general discussion see also Sparks & Chase 2016).

#### 5. FURTHER MODELING CONSIDERATIONS

A primary reason for modeling and simulating filtration is to guide the design of better filters. From the point of view of network modeling, one can ask which characteristics of the pore network are most important in optimizing the outcomes of filtration, suitably defined (for example, maximizing the total filtrate that can be processed by a filter during its useful lifetime, subject to some constraint on the purity of the filtrate). In the following sections, we comment briefly on some important issues.

#### 5.1. Statistical Considerations

Unless working with regular networks such as those in Figure 2c, the process of graph generation is inherently random, and the question of how such randomness (often mirrored in filter membrane manufacture processes) affects outcomes should be addressed. Moreover, unless one makes (unrealistic) simplifications such as uniform pore size, the statistics of pore-size variations should also be considered. The types of model for flow and fouling discussed in Sections 3.2 and 4.1 are sufficiently simple that entire filtration processes on many large networks (say, 1,000 networks of the type shown in **Figure 2***e*) can be simulated in approximately 20 min with modest computing resources (parallelized to, say, 10 processors), allowing one to easily gather reliable statistics on network variations. Similarly, one can fairly efficiently obtain statistics on the influence of poresize variations on a given network. However, gathering statistics on many pore-size samples across many networks, while possible, is still somewhat prohibitive computationally, especially if one is interested in probing network design for optimizing performance. Gu et al. (2022b) made some progress in this direction, investigating separately the effect of network variations (simulations across many networks, with pore sizes in each network drawn from a specified random distribution) and what they call noise variations, in which they take a single typical network and subject it to many statistical realizations of pore-size variations. A key finding is that, provided one controls for network porosity [which has been shown to be a very strong determinant of membrane filter performance (Gu et al. 2022a)], network variations influence filtration outcomes much more strongly than pore-size variations.

## 5.2. Pore Network Design

There are many features of pore network design that are known to impact filtration outcomes and others that have yet to be fully investigated. As noted above, the overall porosity of the pore network is known to be a strong determinant of filter performance, correlating positively with



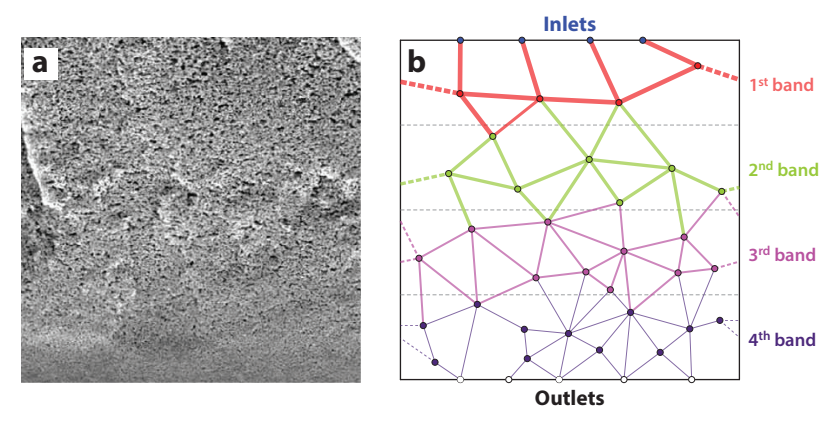


Figure 5

(a) Experimental image (cross section) of a pore-size graded filter. Panel reproduced with permission from Kosiol et al. (2018). (b) Schematic of a simple network with a discrete pore-size gradient. Edges are color-coded to represent pores of different radii, with the edge thickness proportional to the pore radius (dashed edges represent a periodic connection metric). In this example, there is a pore-size gradient but no porosity gradient; hence, where pores are smaller they are more numerous. Panel adapted with permission from Gu et al. (2023).

total filtrate throughput over the filter lifetime and negatively with the purity of the obtained filtrate (Gu et al. 2022a). Pore-size gradients (see **Figure 5**) and/or porosity gradients are also widely known to strongly influence the outcome of filtration, and both have been considered in the context of network modeling (Griffiths et al. 2020, Gu et al. 2023), with model results confirming that moderate negative gradients in either (in the direction of filtrate flow) lead to improved performance.

The role of tortuosity (defined as the average normalized path length taken by fluid traveling through the pore network) in filtration has also been considered. Griffiths et al. (2020) studied the dynamic evolution of pore network tortuosity during the course of filtration, finding that networks become more tortuous as filtration proceeds and that this increase in tortuosity corresponds to improved particle-removal efficiency. Gu et al. (2022a,b) took a different, design-focused approach, studying how the initial tortuosity of a pore network correlates with overall performance. Consistent with the results of Griffiths et al. (2020), particle-removal efficiency was found to correlate strongly with network tortuosity (Gu et al. 2022a). These observations lead one to wonder whether a study of topological features of the pore network could be useful to gain additional insight into filtration efficiency. This is discussed further in Section 6.

## 5.3. Multiple Particle Types or Sizes

Most filtration processes involve feed solutions that carry a variety of different particle types and/or sizes. However, the majority of the modeling in the context of pore networks considers monodisperse feeds. While polydisperse feeds have been discussed fairly extensively from an experimental and computational perspective (Iliev et al. 2015, Sparks & Chase 2016, Wiegmann 2024), little has been done within the context of pore network modeling. Notable recent work includes that of Krupp et al. (2017), who formulate a very general stochastic network model that can account for multiple pore and particle sizes and multiple blocking mechanisms. However, these authors only present simulations for monodisperse feeds on networks, the case of polydisperse feeds being too computationally demanding.

#### 6. OUTLOOK

There are multiple directions in which the field of filtration networks could develop further. One direction that we envision will receive significant traction in the near future emerges from the more general body of work involving flow through porous media networks, but with the additional complexity due to the media's evolution toward clogging as the filtration process proceeds. A plethora of approaches involving analysis of (weighted) networks is possible [see, e.g., the book by Newman (2018)], and we discuss some of them below. In the context of porous media modeling, we briefly review a few approaches that have already been found useful, as well as approaches that we expect to be considered in the near future. In this context, and to emphasize the relevance of such future directions, we note experimental work by Culp et al. (2021) that has revealed a significant influence of the pore-size distribution of the filter medium on the quality of water purification. This work emphasizes that the details of pore networks that go beyond macroscopic measures, such as porosity or permeability, are important. Consistent understanding can be found in recent modeling and computational work (Gu et al. 2022b); however, much more could and should be done.

Several promising approaches are outlined in the book by Korvin (2024); although the focus here is on rock physics, several of the outlined methods are relevant to many other porous media, including filtration pore networks. Korvin (2024, chapter 3), in particular, discusses some novel mathematical techniques, including approaches based on persistent homology (see also Rocks et al. 2021, 2020; Suzuki et al. 2021; Porter et al. 2023) that we discuss further below. The influence of connectivity of pores on the permeability of the porous media was also considered (Griffiths et al. 2016, Alim et al. 2017); in the latter work, the authors find that local pore-size correlations play a significant role, in conjunction with the connectivity, in determining the flow through a porous medium. One step closer in terms of relevance to filtration, flows of suspensions, with particle deposition occurring, were considered experimentally through 3D pore networks (Bizmark et al. 2020) and more recently in the context of flow through an effective 2D model pore network system consisting of closely packed glass beads (Kelly et al. 2023), via both experiments and simulations. These systems have the advantage that confocal microscopy can be used to directly image the deposition of colloidal particles within the pores. An important and perhaps surprising observation is that the applied pressure drop significantly modifies the deposition of the transported particles: If the pressure drop is too large, then the region over which particle deposition occurs is greatly extended, even while the pore network maintains its integrity. A natural question is, To what extent do these findings translate to general filtration pore networks, with implications for purity of the filtrate at elevated pressures?

In the specific context of filtration, an important aspect that must be captured if models and simulations are to be accurate is that the pores composing the networks have a distribution of sizes (Johnston 1998, Alim et al. 2017, Gu et al. 2022b), giving rise to a weighted network. Pore length distributions arise naturally from the chosen network generation method, while pore radii (if modeled as circular cylinders) are usually assigned according to some distribution and furthermore are evolving, raising the question of how to appropriately describe such evolution. We consider persistent homology (mentioned above; see Korvin 2024) to be promising in this context, since it allows for the formulation of precise measures that quantify the network evolution. Such measures were usefully considered in the context of granular systems (Kramár et al. 2013, 2014a) and for flow networks relevant to the circulatory system (Ronellenfitsch & Katifori 2019), leaf veins (Ronellenfitsch et al. 2015), microvascular networks (Chang & Roper 2019), shale matrix gas flows (Mehmani et al. 2013), and river estuaries (Konkol et al. 2022); we therefore expect that they will also find fruitful application in the context of classifying effective filtration networks.



A valuable feature of the measures emerging from persistent homology is that they offer a reduced representation of a (potentially very large) network in the form of persistence diagrams (PDs) [see, e.g., the paper by Kramár et al. (2014b) or the accessible review article by Porter et al. (2023)]. These diagrams have certain essential features that make them potentially useful tools. One is that they provide a significant data reduction, allowing the compact and efficient storage of information about large, time-dependent networks, while still retaining a significant part of the information related to the connectivity and topology of the networks. PDs are typically generated via some thresholding process on the selected dataset; in a network with a distribution of pore sizes, the pore radius provides a convenient threshold parameter by which to track topology. In superlevel thresholding, the pore radius threshold is decreased from the maximum radius down to the minimum, and topological features (individual pores, simply connected subnetworks, loops and holes) appear, and possibly disappear (merge), in the process. PDs record the birth and death of such features as thresholding proceeds, the total lifetime of a feature (with respect to the threshold range) being a measure of its topological importance or persistence. The number of PDs that can be constructed for variable-radii networks is equal to the number of physical dimensions; such PDs give rise to compact measures such as total persistence (TP), a simple aggregate measure of the lifetimes of all such features (see Kramár et al. 2014b). Preliminary investigations suggest that even such simple measures may show quite strong correlations with filtration performance metrics (for an example of TP corresponding to loops/cycles in a filtration network, see Figure 6).

A second helpful feature is that PDs provide a convenient interface to various ML computing approaches (see, e.g., Liu et al. 2024). While it is not necessary to use PDs to explore the application of ML to filtration networks, the convenience of using such an approach will, we believe, find significant relevance in the near future. ML has already been implemented by several groups with the goal of correlating the properties of porous media to the performance in a particular application (usually measured in terms of permeability). Such progress has been discussed in recent reviews by Wang et al. (2021) and Yang et al. (2024). The outlined approaches typically start from experimental or synthetic data, which are then either used as input to large-scale simulations or reduced to corresponding effective networks, which could then again be used as a basis for

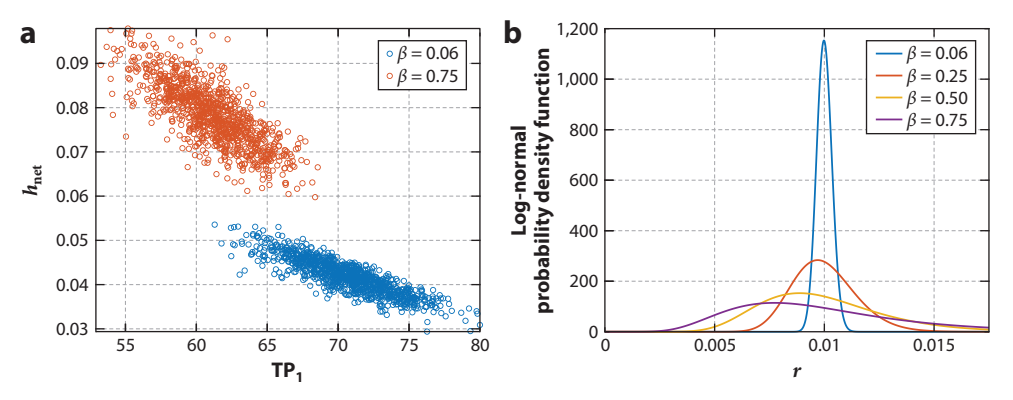


Figure 6

(a) Preliminary results (unpublished) showing strong correlations between the total filtrate processed by a filter over its lifetime ( $b_{net}$ ); the subscript indicates that each dot corresponds to a different network, 1,000 networks in total, and the total persistence (TP<sub>1</sub>) associated with loops for each network. Each of the 1,000 networks has its pore radii drawn from a single set of (randomly assigned) pore radii emerging from the log-normal pore radius distribution, while fixing the overall porosity to  $\phi = 0.6$ . Two pore radius distributions are investigated, indicated by the  $\beta$ -values. (b) The pore radius probability distribution functions for selected  $\beta$ -values (all pore radii are normalized by the total membrane thickness).

simulations, with the ultimate goal of correlating material structure to performance (permeability). ML can be used in various forms to assist with or guide all stages of this process. One of several interesting works in this direction, using synthetic data, is the work by Röding et al. (2020), who use multiple descriptors of porous media with the goal of predicting permeability based on the porous material structural information. In the context of filtration pore networks, we see a few emerging questions that could, and perhaps should, be considered using ML: How can the geometry and topology of a filtration network be optimized to provide the best outcome (given specified constraints)? What are the most essential properties of the filtration pore networks that determine the outcome?

While persistence homology provides a robust framework for capturing the evolution of topological features in dynamic graphs, the underlying flow network structure offers a complementary perspective for deriving effective medium approximations. The setup of flow networks enables the application of asymptotic homogenization to derive effective medium equations that govern net fluid flow, species transport, and permeability evolution. Two primary continuum limits are typically considered: increasing the number of nodes to infinity and reducing the interconnectivity distance between nodes (to zero). Calder (2024), for instance, demonstrates several techniques for deriving effective equations under these continuum limits for problems on static graphs, and Chapman & Wilmott (2021) perform homogenization over a periodic spatial domain within a pore network by employing a discrete version of the method of multiple scales to derive expressions for effective permeability and network tortuosity. A natural direction for future work is to extend these methods to dynamic temporal graphs, which more accurately represent real networks in practical applications and engineering contexts. Additionally, when incorporating sieving as a fouling mechanism—often modeled as a stochastic process—one can approximate the state of each pore (open or closed) by analytically calculating the probability of blocking events using classical Markov chain theory (for a flavor of this type of argument, see Hoffmann et al. 2013). Such analytical treatment eliminates the need for stochastic simulations in linear problems (or provides a first-order approximation for nonlinear problems), creating computational savings that can be leveraged to systematically explore other forms of stochasticity, such as variations in pore-size and particle-size distributions.

This outlook places the flow and particle deposition within filtration pore networks in a wider context that extends from porous media flow to the large field of complex weighted networks that is relevant in a number of contexts. We expect that, driven by industrial demand, the field of filtration modeling will continue to grow at the interface of these related fields in the years and decades to come.

#### **SUMMARY POINTS**

- The pore structure of many classes of porous materials can be reasonably approximated as a network of interconnected pores.
- 2. Network theory and the Hagen–Poiseuille flow model then provide a robust and computationally efficient framework for modeling flow through such porous media.
- 3. For filtration applications, fluid dynamics must be coupled to a model for particle transport and deposition (fouling) within the pores, leading to an evolving network.
- 4. For accurate predictions of filter efficiency and lifetime, the pore network evolution under fouling must be correctly modeled.

#### **FUTURE ISSUES**

- While diffusive effects have been implemented in computationally intensive models and via reduced modeling for single-pore models, they have yet to be implemented efficiently on a large-scale network model. Such implementation will require efficient methods for solving partial differential equations on large networks.
- Shielding effects may have important implications for how filter efficiency changes over time and should be further considered.
- 3. Integrated models that can simultaneously account for adsorptive and blocking fouling on large networks should be developed.
- 4. In our opinion, methodology from topological data analysis and machine learning shows significant potential and should be further explored for efficient filter design investigations.
- 5. Homogenization theory is likewise viewed as a promising area for further development.

#### **DISCLOSURE STATEMENT**

The authors are not aware of any affiliations, memberships, funding, or financial holdings that might be perceived as affecting the objectivity of this review.

#### **ACKNOWLEDGMENTS**

L.J.C. and L.K. acknowledge funding from the National Science Foundation (NSF) under grant NSF DMS 2206127.

#### LITERATURE CITED

Abdallah A, Vincens E, Magoariec H, Picault C. 2023. DEM filtration modelling for granular materials: comparative analysis of dry and wet approaches. Int. J. Numer. Anal. Methods Geomech. 48(3):870–86

Abdoli SM, Shafiei S, Raoof A, Ebadi A, Jafarzadeh Y, Aslannejad H. 2018. Water flux reduction in microfiltration membranes: a pore network study. Chem. Eng. Technol. 41:1566–76

Alim K, Parsa S, Weitz DA, Brenner MP. 2017. Local pore size correlations determine flow distributions in porous media. *Phys. Rev. Lett.* 119:144501

Apel P. 2001. Track etching technique in membrane technology. Radiat. Meas. 34:559-66

Arioli M, Benzi M. 2018. A finite element method for quantum graphs. IMA J. Num. Anal. 38:1119-63

Bear J. 1972. Dynamics of Fluids in Porous Media. Elsevier

Berkolaiko G, Kuchment P. 2013. Introduction to Quantum Graphs. American Mathematical Society

Beuscher U. 2010. Modeling sieving filtration using multiple layers of parallel pores. *Chem. Eng. Technol.* 33:1377-81

Bizmark N, Schneider J, Priestley RD, Datta SS. 2020. Multiscale dynamics of colloidal deposition and erosion in porous media. Sci. Adv. 6:eabc2530

Blunt MJ, Bijeljic B, Dong H, Gharbi O, Iglauer S, et al. 2013. Pore-scale imaging and modelling. *Adv. Water Resour.* 51:197–216

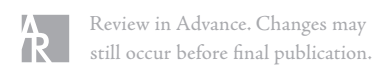
Boussu K, Zhang Y, Cocquyt J, Van der Meeren P, Volodin A, et al. 2006. Characterization of polymeric nanofiltration membranes for systematic analysis of membrane performance. *J. Membr. Sci.* 278:418–27

Brio M, Caputo JG, Kravitz H. 2022. Spectral solutions of PDEs on networks. *Appl. Num. Math.* 172:99–117

Caglar B, Broggi G, Ali M, Orgeas L, Michaud V. 2022. Deep learning based prediction of fibrous microstructure permeability. In ECCM 2022 - Proceedings of the 20th European Conference on Composite Materials: Composites Meet Sustainability, ed. A Vassilopoulos, V Michaud. Elsevier

www.annualreviews.org • Filtration Networks

- Calder J. 2024. The calculus of variations. Notes. https://www-users.cse.umn.edu/wcalder/CalculusOfVariations.pdf
- Chaipetch W, Jaiyu A, Jutaporn P, Heran M, Khongnakorn W. 2021. Fouling behavior in a high-rate anaerobic submerged membrane bioreactor (AnMBR) for palm oil mill effluent (POME) treatment. *Membranes* 11:649
- Chang SS, Roper M. 2019. Microvascular networks with uniform flow. J. Theoret. Biol. 462:48-64
- Chapman SJ, Wilmott ZM. 2021. Homogenisation of flow through periodic networks. SIAM J. Appl. Math. 81(3):1034–51
- Chen S, Doolen GD. 1998. Lattice Boltzmann method for fluid flows. Annu. Rev. Fluid Mech. 30:329-64
- Culp TE, Khara B, Brickey KP, Geitner M, Zimudzi TJ, et al. 2021. Nanoscale control of internal inhomogeneity enhances water transport in desalination membranes. *Science* 371(6524):72–75
- Darcy H. 1856. Les fontaines publiques de la ville de Dijon. Dalmont
- Dincau B, Dressaire E, Sauret A. 2023. Clogging: the self-sabotage of suspensions. Phys. Today 76:24-30
- Dressaire E, Sauret A. 2017. Clogging of microfluidic systems. Soft Matter 13(1):37-48
- Esser S, Löwer E, Peuker UA. 2021. Network model of porous media review of old ideas with new methods. Sep. Purif. Technol. 257:117854
- Fallahianbijan F, Giglia S, Carbrello C, Zydney AL. 2017. Use of fluorescently-labeled nanoparticles to study pore morphology and virus capture in virus filtration membranes. J. Membr. Sci. 536:52–58
- Fatt I. 1956a. The network model of porous media I. Capillary pressure characteristics. *AIME Petrol. Trans.* 207:144–59
- Fatt I. 1956b. The network model of porous media II. Dynamic properties of a single size tube network. AIME Petrol. Trans. 207:160–63
- Fatt I. 1956c. The network model of porous media III. Dynamic properties of networks with tube radius distribution. AIME Petrol. Trans. 207:164–81
- Gavrilchenko T, Katifori E. 2018. Resilience in hierarchical fluid flow networks. Phys. Rev. E 99(1):012321
- Gong L, Nie L, Xu Y. 2020. Geometrical and topological analysis of pore space in sandstones based on X-ray computed tomography. *Energies* 13:3774
- Goodman RH, Conte G, Marzuola JL. 2024. QGlab: a MATLAB package for computations on quantum graphs. SIAM J. Sci. Comput. 47(2):B428–53
- Grady LJ. 2010. Discrete Calculus: Applied Analysis on Graphs for Computational Science. Springer
- Griesser A, Fingerle M. 2020. AI based 3D image analysis with GeoDict. Microsc. Microanal. 26(S2):518-19
- Griffiths IM, Kumar A, Stewart PS. 2014. A combined network model for membrane fouling. J. Coll. Int. Sci. 432:10–18
- Griffiths IM, Kumar A, Stewart PS. 2016. Designing asymmetric multilayered membrane filters with improved performance. *7. Membr. Sci.* 511:108–18
- Griffiths IM, Mitevski I, Vujkovac I, Illingworth MR, Stewart PS. 2020. The role of tortuosity in filtration efficiency: a general network model for filtration. *J. Membr. Sci.* 598:117664
- Gu B, Kondic L, Cummings L. 2022a. A graphical representation of membrane filtration. SIAM J. Appl. Math. 82:950–75
- Gu B, Kondic L, Cummings L. 2022b. Network-based membrane filters: influence of network and pore size variability on filtration performance. J. Membr. Sci. 657:120668
- Gu B, Kondic L, Cummings LJ. 2023. Flow through pore-size graded membrane pore network. Phys. Rev. Fluids 8(4):044502
- Gu B, Renaud DR, Sanaei P, Kondic L, Cummings LJ. 2020. On the influence of pore connectivity on performance of membrane filters. J. Fluid Mech. 902:A5
- Herterich J, Griffiths I, Vella D. 2019. Reproducing the pressure–time signature of membrane filtration: the interplay between fouling, caking, and elasticity. *J. Membr. Sci.* 577:235–48
- Ho CC, Zydney AL. 2000. A combined pore blockage and cake filtration model for protein fouling during microfiltration. 7. Coll. Int. Sci. 232(2):389–99
- Hoffmann T, Porter MA, Lambiotte R. 2013. Random walks on stochastic temporal networks. In *Temporal Networks*, ed. P Holme, J Saramäki. Springer
- Iliev O, Kirsch R, Lakdawala Z, Rief S, Steiner K. 2015. Modeling and simulation of filtration processes. In *Currents in Industrial Mathematics: From Concepts to Research to Education*, ed. H Neunzert, D Prätzel-Wolters. Springer
- 242 Cummings Gu Kondic



- Iritani E, Katagiri N. 2016. Developments of blocking filtration model in membrane filtration. KONA Powder Part. J. 33:179–202
- Jiang Z, Wu K, Couples G, van Dijke MI, Sorbie KS, Ma J. 2007. Efficient extraction of networks from threedimensional porous media. Water Resour. Res. 43(12):W12S03
- Johnston PR. 1998. Revisiting the most probable pore-size distribution in filter media: the gamma distribution. Filtr. Sep. 35:287
- Kelly G, Bizmark N, Chakraborty B, Datta SS, Fai TG. 2023. Modeling the transition between localized and extended deposition in flow networks through packings of glass beads. *Phys. Rev. Lett.* 130(12):128204
- Kim AS, Liu Y. 2008. Critical flux of hard sphere suspensions in crossflow filtration: hydrodynamic force bias Monte Carlo simulations. *J. Membr. Sci.* 323(1):67–76
- Kiradjiev K, Breward C, Griffiths I, Schwendeman D. 2021. A homogenised model for a reactive filter. SIAM J. Appl. Math. 81:591–619
- Konkol A, Schwenk J, Katifori E, Shaw JB. 2022. Interplay of river and tidal forcings promotes loops in coastal channel networks. *Geophys. Res. Lett.* 49(10):e2022GL098284
- Korvin G. 2024. Statistical Rock Physics. Springer Nature
- Köry J, Krupp A, Please C, Griffiths I. 2021. Optimising dead-end cake filtration using poroelasticity theory. Modelling 2(1):18–42
- Kosiol P, Müller MT, Schneider B, Hansmann B, Thom V, Ulbricht M. 2018. Determination of pore size gradients of virus filtration membranes using gold nanoparticles and their relation to fouling with protein containing feed streams. *J. Membr. Sci.* 548:598–608
- Kramár M, Goullet A, Kondic L, Mischaikow K. 2013. Persistence properties of compressed granular matter. Phys. Rev. E 87:042207
- Kramár M, Goullet A, Kondic L, Mischaikow K. 2014a. Evolution of force networks in dense particulate media. Phys. Rev. E 90:052203
- Kramár M, Goullet A, Kondic L, Mischaikow K. 2014b. Quantifying force networks in particulate systems. *Physica D* 283:37–55
- Krupp A, Griffiths I, Please C. 2017. Stochastic modelling of membrane filtration. *Proc. R. Soc. A* 473:20160948 Lawrie T, Tanner G, Chronopoulos D. 2022. A quantum graph approach to metamaterial design. *Sci. Rep.* 12(1):18006
- Leighton D, Acrivos A. 1987a. Measurement of shear-induced self-diffusion in concentrated suspensions of spheres. J. Fluid Mech. 177:109–31
- Leighton D, Acrivos A. 1987b. The shear-induced migration of particles in concentrated suspensions. J. Fluid Mech. 181:415–39
- Liu J, Shen L, Wei GW. 2024. ChatGPT for computational topology. Found. Data Sci. 6(2):221-50
- Liu SY, Chen Z, Sanaei P. 2020. Effects of particles diffusion on membrane filters performance. Fluids 5(3):121
- Marin A, Souzy M. 2025. Clogging of noncohesive suspension flows. Annu. Rev. Fluid Mech. 57:89-116
- Mehmani A, Prodanović M, Javadpour F. 2013. Multiscale, multiphysics network modeling of shale matrix gas flows. *Transport Porous Media* 99(2):377–90
- Newman M. 2018. Networks. Oxford University Press
- Park JA, Nam A, Kim JH, Yun ST, Choi JW, Lee SH. 2018. Blend-electrospun graphene oxide/Poly(vinylidene fluoride) nanofibrous membranes with high flux, tetracycline removal and anti-fouling properties. Chemosphere 207:347–56
- Pereira VE, Dalwadi MP, Griffiths IM. 2021. Role of caking in optimizing the performance of a concertinaed ceramic filtration membrane. *Phys. Rev. Fluids* 6(10):104301
- Porter MA, Feng M, Katifori E. 2023. The topology of data. Phys. Today 76(1):36-42
- Probstein RF. 1994. Physicochemical Hydrodynamics. Wiley-Interscience
- Rege SD, Fogler HS. 1987. Network model for straining dominated particle entrapment in porous media. *Chem. Eng. Sci.* 42(7):1553–64
- Ridgway CJ, Gane PA, Schoelkopf J. 2002. Effect of capillary element aspect ratio on the dynamic imbibition within porous networks. *J. Coll. Int. Sci.* 252(2):373–82
- Rocks JW, Liu AJ, Katifori E. 2020. Revealing structure-function relationships in functional flow networks via persistent homology. Phys. Rev. Res. 2(3):033234

www.annualreviews.org • Filtration Networks



- Rocks JW, Liu AJ, Katifori E. 2021. Hidden topological structure of flow network functionality. Phys. Rev. Lett. 126(2):028102
- Röding M, Ma Z, Torquato S. 2020. Predicting permeability via statistical learning on higher-order microstructural information. Sci. Rep. 10(1):15239
- Ronellenfitsch H, Katifori E. 2019. Phenotypes of vascular flow networks. Phys. Rev. Lett. 123(24):248101
- Ronellenfitsch H, Lasser J, Daly DC, Katifori E. 2015. Topological phenotypes constitute a new dimension in the phenotypic space of leaf venation networks. *PLOS Comput. Biol.* 11(12):e1004680
- Ruiz-García M, Katifori E. 2021. Emergent dynamics in excitable flow systems. Phys. Rev. E 103(6):062301
- Sanaei P, Cummings LJ. 2017. Flow and fouling in membrane filters: effects of membrane morphology. J. Fluid Mech. 818:744–71
- Sanaei P, Cummings LJ. 2018. Membrane filtration with complex branching pore morphology. Phys. Rev. Fluids 3:094305
- Sanaei P, Cummings LJ. 2019. Membrane filtration with multiple fouling mechanisms. *Phys. Rev. Fluids* 4:124301
- Sanaei P, Richardson GW, Witelski T, Cummings LJ. 2016. Flow and fouling in a pleated membrane filter. 7. Fluid Mech. 795:36–59
- Schoelkopf J, Gane PAC, Ridgway CJ, Matthews GP. 2002. Practical observation of deviation from Lucas– Washburn scaling in porous media. Colloids Surfaces A Physicochem. Eng. Aspects 206(1):445–54
- Shi C, Janssen H. 2025. Improved algorithm for stochastic pore network generation for porous materials. Transp. Porous Media 152(5):33
- Simon R, Kelsey F. 1971. Use of capillary tube networks in reservoir performance studies: I. Equal-viscosity miscible displacements. Soc. Petrol. Eng. J. 11(2):99–112
- Song Q, Lin Y, Gan N, Sadam H, An Y, et al. 2025. Ultrathin surface-amination-modified membrane with ion-charge shielding effect for ultraselective nanofiltration. *Desalination* 597:118325
- Sparks T, Chase G. 2016. Filters and Filtration Handbook. Butterworth-Heinemann. 6th ed.
- Sutera SP, Skalak R. 1993. The history of Poiseuille's law. Annu. Rev. Fluid Mech. 25:1-20
- Suzuki A, Miyazawa M, Minto JM, Tsuji T, Obayashi I, et al. 2021. Flow estimation solely from image data through persistent homology analysis. Sci. Rep. 11(1):17948
- Taira K, Nair AG. 2022. Network-based analysis of fluid flows: progress and outlook. Prog. Aerosp. Sci. 131:100823
- Tanudjaja HJ, Anantharaman A, Ng AQQ, Ma Y, Tanis-Kanbur MB, et al. 2022. A review of membrane fouling by proteins in ultrafiltration and microfiltration. *J. Water Proc. Eng.* 50:103294
- The MathWorks Inc. 2024. MATLAB, Version 9.13.0 (r2022b). https://www.mathworks.com/products/matlab.html
- van Reis R, Zydney A. 2001. Membrane separations in biotechnology. *Curr. Opin. Biotechnol.* 12(2):208–11 van Reis R, Zydney A. 2007. Bioprocess membrane technology. *J. Membr. Sci.* 297(1):16–50
- Wang YD, Blunt MJ, Armstrong RT, Mostaghimi P. 2021. Deep learning in pore scale imaging and modeling. Earth-Sci. Rev. 215:103555
- Wiegmann A. 2024. GeoDict. Kaiserslautern. https://www.geodict.com
- Xiong Q, Baychev TG, Jivkov AP. 2016. Review of pore network modelling of porous media: experimental characterisations, network constructions and applications to reactive transport. J. Contam. Hydrol. 192:101–17
- Yang G, Xu R, Tian Y, Guo S, Wu J, Chu X. 2024. Data-driven methods for flow and transport in porous media: a review. Int. J. Heat Mass Trans. 235:126149
- Zhang B, Zhang R, Huang D, Shen Y, Gao X, Shi W. 2020. Membrane fouling in microfiltration of alkali/surfactant/polymer flooding oilfield wastewater: effect of interactions of key foulants. J. Coll. Int. Sci. 570:20–30
- Zhang J, Hoshino K. 2018. Molecular Sensors and Nanodevices: Principles, Designs and Applications in Biomedical Engineering. Elsevier. 2nd ed.
- Zydney AL, Aimar P, Meireles M, Pimbley JM, Belfort G. 1994. Use of the log-normal probability density function to analyze membrane pore size distributions: functional forms and discrepancies. *J. Membr. Sci.* 91:293–98